

## RESEARCH ARTICLE

10.1002/2015JF003656

## Investigating decadal-scale geomorphic dynamics in an alpine mountain setting

## Key Points:

- Archival aerial imagery to investigate decadal-scale changes
- Distinct response to different climatic forcing periods
- Geomorphic change investigation

## Correspondence to:

N. Micheletti,  
natan.micheletti@unil.ch

## Citation:

Micheletti, N., C. Lambiel, and S. N. Lane (2015), Investigating decadal-scale geomorphic dynamics in an alpine mountain setting, *J. Geophys. Res. Earth Surf.*, 120, doi:10.1002/2015JF003656.

Received 25 JUN 2015

Accepted 22 SEP 2015

Accepted article online 24 SEP 2015

Natan Micheletti<sup>1</sup>, Christophe Lambiel<sup>1</sup>, and Stuart N. Lane<sup>1</sup><sup>1</sup>Institute of Earth Surface Dynamics, University of Lausanne, Lausanne, Switzerland

**Abstract** We know little about the effect of recent climate variability upon landscapes at the timescale of decades because of (1) the complex, nonlinear, and path-dependent nature of the response of a landscape to climate forcing and (2) the difficulty of quantifying spatially distributed impacts at the timescale of decades to centuries, despite this being the timescale over which significant hypotheses have been raised over human impacts upon climate change and hence geomorphic systems. A unique resource to investigate the linkages between climatic variability and geomorphic response is provided by the extensive coverage of aerial imagery commonly available since the 1950s. Here we use archival digital photogrammetry to produce high-precision digital elevation models over large spatial scales, and so to reconstruct the quantitative history of surface downwasting and sediment flux in a high mountain alpine system, over the timescales of decades. Propagation of error methods is used to identify locations of significant landscape response and to compute volumes of significant surface change. Orthorectified aerial images are used in an image correlation framework to detect horizontal and vertical displacements of components of the landscape. Results are coupled to extant climate data and modeled snow cover to show how the landscape responds to climate forcing and to geomorphological maps to understand how this response varies between landscape elements. The results show distinct landscape response to both warming and cooling periods and a tendency for the acceleration of surface displacement under warming conditions. Precipitation and snow cover are critical in controlling glacier dynamics and rock glacier displacement velocities. However, while some landforms might lead to locally high sediment flux, landscape heritage can disconnect zones of high change rates from the valley bottom. Hence, the landscape response to climate forcing is not necessarily reflected in valley system processes or sediment deposits.

## 1. Introduction

A progressive refinement of our understanding of climate change patterns has followed from the first and subsequent state-of-the-art syntheses of human impact on climate provided by the *Intergovernmental Panel on Climate Change* [1990], contributing fundamentally to our knowledge about how climate might change in the future. Despite this, quantification of climate change impacts upon the Earth system is underdeveloped [Kundzewicz et al., 2007], not least because of the complex, nonlinear response of geomorphic systems to perturbations [Phillips, 2003, 2009] and the difficulties of quantifying this response over large spatial and long temporal scales. While this is generally valid, it is especially true for polar, glacial, and periglacial regions which are potentially more vulnerable to climate change [Committee on Challenges and Opportunities in Earth Surface Processes, 2010]. The high climatic sensitivity of high mountain environments follows from four points. First, the glaciers, permafrost, and nival processes that are widely present in these landscapes are highly sensitive to changes in atmospheric temperature [Pelto and Hedlund, 2001; Kääb et al., 2007; Carturan et al., 2013; Oliva and Ruiz-Fernandez, 2015; Staines et al., 2015]. Second, glaciated environments typically have increased relief, the steep slopes potentially aiding sediment mobilization [Brocklehurst and Whipple, 2002]. Third, deglaciated mountain environments commonly have significant amounts of historically weathered and glacially derived material, and so a legacy of high sediment availability [Ballantyne et al., 2014]. Finally, sediment dynamics are strongly dependent upon the thermal state of the subsurface, in terms of both sediment stabilization and production [Davies et al., 2001; Hales and Roering, 2007] and surface runoff generation because of the presence/absence of impeded drainage [Ford and Bedford, 1987; Bayard et al., 2005].

Understanding how climate change affects sediment production, transfer, and delivery in mountain landscapes is a fundamental focus of current geomorphic research [Montgomery and Stover, 2001; Hunt, 2002;

*Jomelli et al., 2004; Korup, 2004; Lane et al., 2007*). Scientific observations suggest that high mountain environments could be very sensitive to climate change, and an acceleration in sediment production and transport rates has been reported for some landforms in mountain sedimentary systems [*Warner, 1987; Rumsby and Macklin, 1994; Dollar and Rowntree, 1995; Knox, 1999; Jomelli et al., 2004; Roer et al., 2008; Huggel et al., 2010, 2012; Bennett et al., 2013*]. However, increased sediment delivery and transport for single landforms does not necessarily imply a climatic response at the landscape scale as (1) a landscape may contain a range of different landforms each with different climate sensitivities [*Brunsdon and Thornes, 1979*] and (2) connection between these elements will be the ultimate control on sediment delivery. Effectively, a lack of sediment flux between landforms and sediment storage zones may lead to disconnections in parts of the sediment cascade [*Brunsdon and Thornes, 1979; Fryirs, 2013*]. This may slow, or even halt, the diffusion of climate impacts through hillslopes. A large number of studies have considered climate forcing of single-landform types [*Hölzle and Haeberli, 1995; Jomelli et al., 2004; Huggel et al., 2010, 2012*]. Yet, it is the connections between them that determine whether or not sediment transfer rates will respond to climate change [*Reynard et al., 2012*].

This contribution addresses two research questions that follow from the above. First, are there coincidences between changes in climate forcing and modifications in alpine geomorphic process patterns and rates? Second, as the diffusion of the effects of such forcing may depend on the connections between individual landforms, can we see any evidence of the propagation of climate signals through the landscape? In order to respond to these questions we investigate the behavior of high mountain environments at a timescale of years to decades. A unique resource for such investigation is the extensive coverage of aerial imagery commonly available since the 1950s, which can be employed to produce high-precision digital elevation models (DEMs) over large spatial scales using digital photogrammetry. Research has demonstrated the potential of this approach for geomorphological studies including fluvial geomorphology [*Lane et al., 2003, 2010; Hughes et al., 2006*], mountain geomorphology [*Kääb and Vollmer, 2000; Kääb, 2002; Wangenstein et al., 2006; Kneisel and Kääb, 2007; Fischer et al., 2011, 2012; Roer et al., 2005*] and studies of hillslope processes and sediment production, transfer, and yield [*Chandler and Cooper, 1988; Walstra et al., 2007; Schwab et al., 2008; Bennett et al., 2012, 2013*]. Our focus is upon a case study in the Swiss Alps, typical of many alpine mountain regions, where there is a range of landforms juxtaposed within the landscape. Aerial imagery from the 1960s to present is used to compute high-precision and fine-resolution digital elevation models. A quantitative comparison of successive DEMs employing propagation of error methods is implemented to identify locations of significant elevation change and geomorphic response and to estimate volumes of erosion and deposition and of glacier growth and retreat. To identify mass displacement, the derived orthorectified images are used in an image correlation framework to visualize and quantify surface displacements and their velocities over time. Results are coupled to extant climate data and modeled snow depth to show how the landscape responds to climate forcing and to geomorphological maps to understand how this response varies between both landforms and their spatial organization. Finally, given the possibly important role of sediment supply and connectivity in propagating the climatic signal through the hillslope, an attempt to identify how connectivity might impact fluxes to the valley bottom is undertaken.

## 2. Study Site

The focus of this investigation is the Veisivi-Tsa ridge in the Hérens Valley, Switzerland (Figure 1). This steep alpine mountainside has an elevation range from 1800 m above sea level (asl) to 3676 m asl and an average slope of  $\sim 35^\circ$ . The basin extends for  $\sim 5$  km north-south, between the Petit Dent de Veisivi (3184 m asl) and La Maya (3042 m asl). The region is relatively dry because of the topographic barrier effect of the southern alpine divide, with annual precipitation between 900 and 1300 mm and mean annual air temperature at 2000 m asl of  $3.4^\circ\text{C}$  based upon the period 1991 to 2014 *Meteosuisse* [2014]. The geomorphological setting of the landscape comprises an assemblage of glacial, periglacial, hillslope, and fluvial landforms and a complete range of primary sediment transfer mechanisms, typical of alpine environments. The area has been the subject of previous geomorphological investigations, especially regarding permafrost distribution and quantification of slope movement using interferometric synthetic aperture radar (InSAR) [*Lambiel et al., 2004, 2008; Delaloye et al., 2007, 2008, 2010; Barboux et al., 2014*].

## 3. Methodology

The methods used to generate the DEMs and orthophotographs used in this study are presented in an accompanying methods paper [*Micheletti et al., 2015*], and only a summary is provided here.

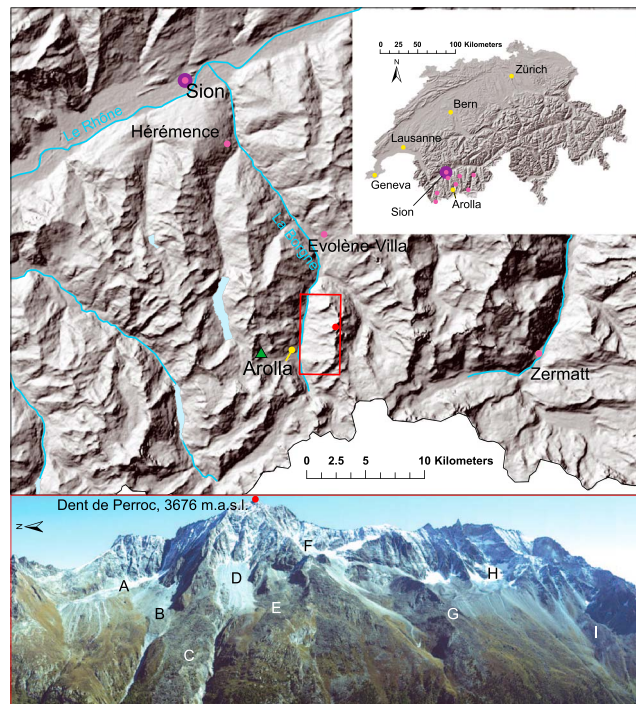


**Figure 1.** The Veisivi-La Tsa ridge case study in Arolla, Hérens Valley, Switzerland (relief shaded and river data: Swisstopo) with sites of interest: Tsarmin glacier (A), Tsarmin rock glacier (B), Perroc rockslide (C), Perroc talus slope (D), Lé Blâva rock glacier (E), Genevois glacier (F), La Tsa hut (G), La Tsa glacier (H), and La Roussette rock glacier (I).

### 3.1. Digital Elevation Models and Interpretation

The archival aerial imagery employed in this study was acquired by the Swiss Federal Office of Topography (Swisstopo, [www.swisstopo.admin.ch](http://www.swisstopo.admin.ch)) and by Flotron AG ([www.flotron.ch](http://www.flotron.ch)). Swisstopo imagery includes a number of  $23 \times 23$  cm images for seven distinct epochs between 1967 and 2005 all collected at similar periods of the year (end of summer or beginning of autumn) at altitudes varying between 5000 and 7000 m asl and using a range of analogue cameras. A photogrammetric quality scanner was used to scan these images at  $14 \mu\text{m}$  (1814 dpi). These images vary in scale between 1:15,700 and 1:28,000. Calibration certificates for analogue cameras were available at [www.swisstopo.admin.ch](http://www.swisstopo.admin.ch). It should be noted that the 1977 imagery was collected during partially snow-covered conditions, and hence the derived data quality are lower for that year. Flotron AG images were collected in September 2012 using an UltraCam-X camera, and they represent the most recent data set of the study. They are composed of  $14,430 \times 9420$  pixels of  $7.2 \mu\text{m}$  and have a scale of 1:5200. Multiple images were required to cover the whole area of interest. The Flotron AG digital imagery was provided with a calibration file for the digital camera.

In order to obtain the required ground control points (GCPs) necessary for photogrammetric restitution, a field campaign was carried out in July 2012 using two Leica System 500 differential GPS units. A total of 169 GCPs were identified, stable in time and easily and precisely identifiable on images (Figure 2), across an area of approximately  $20 \text{ km}^2$  ( $3 \times 6.5 \text{ km}$ ) and with an elevation range of more than 1000 m (1808 to 2828 m asl). Original RTK data processing and correction using Automated GNSS Network for Switzerland (AGNES) data allowed the determination of coordinates of all GCPs in the Swiss coordinate system to the geodetic datum CH1903 with a precision better than  $\pm 0.05 \text{ m}$ .

The detailed methodology is presented in full in *Micheletti et al.* [2015]. All photogrammetric data processing was performed using ERDAS IMAGINE Leica Photogrammetry Suite (LPS) 2010, while postprocessing operations and results analysis were implemented using Matlab 2013 and ArcGIS 10. Calibration certificates and GCPs were used to estimate interior and exterior orientation parameters, respectively. Afterward, as is routine in digital photogrammetry [Dissart and Jamet, 1995], an automatic stereomatching algorithm was used to match points in image pairs and to compute their ground coordinates using exterior orientation parameters. Finally, the data were interpolated to generate 1 m resolution raster DEMs for every year. The quality

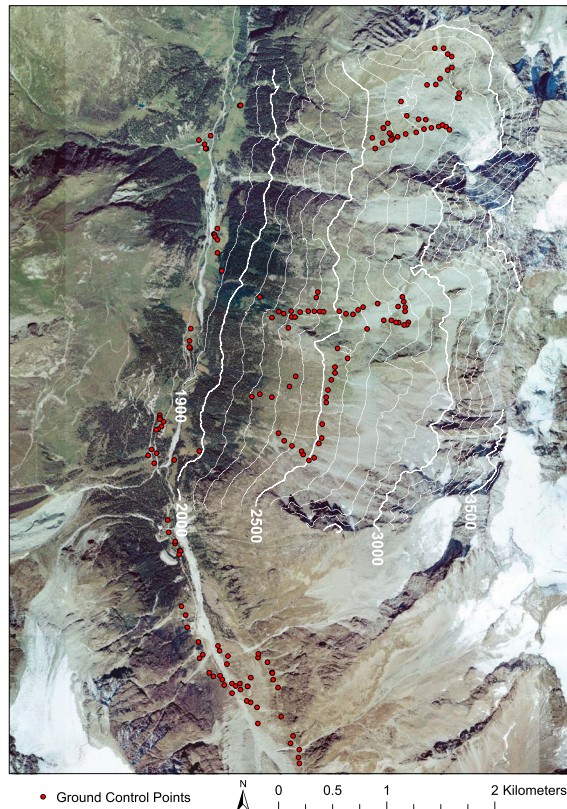


**Figure 2.** Ground control point distribution in the Arolla Valley, Switzerland (contour line spacing: 100 m, orthophoto: Swisstopo 2005).

assessment of individual DEMs was carried out using unused GCPs. As in Lane *et al.* [2000], errors were defined as the differences in elevation between dGPS measurements and the DEM values at corresponding dGPS locations and were used to compute accuracy in the form of mean error (ME) and precision in the form of standard deviation of error (STD) (Table 1). The shape of these error distributions was investigated and confirmed to be Gaussian at the 5% significance level [Micheletti *et al.*, 2015].

DEMs of difference (DoD) were computed by differencing DEMs for different years. This allows identification of changes between dates and hence patterns of erosion and deposition. However, it was necessary to quantify the confidence that apparent changes between two epochs are real and not produced by random error. Following the error propagation methodology proposed in Lane *et al.* [2003] for Gaussian error distributions, the uncertainty in the magnitude of change in the DoD was determined by the root of the sum in quadrature of the uncertainties associated with individual DEMs:

$$\sigma_c = \sqrt{\sigma_1^2 + \sigma_2^2} \tag{1}$$

In this instance, the standard deviation of error is used as a measure of uncertainty, but it can be employed to formulate a statistical testing of the significance of each elevation difference  $z_1 - z_2$  using a *t* test [Lane *et al.*, 2003]:

$$t = \frac{z_1 - z_2}{\sqrt{\sigma_1^2 + \sigma_2^2}} \tag{2}$$

**Table 1.** DEM Precision and Accuracy Assessment Using dGPS Survey Data (m)

DEM	1967	1977	1983	1988	1995	1999	2005	2012
ME	0.315	0.504	0.281	0.296	0.541	0.493	0.453	0.356
STD	±0.765	±0.820	±0.953	±0.644	±0.751	±0.827	±0.998	±0.462

**Table 2.** Limits of Detection of Change (LoD) With a Confidence Limit of 67% and 90% Computed Using the Error Propagation Methods Explained Above (m)

Year Pair	67%	90%
2012–2005	1.100	1.804
2005–1999	1.296	2.126
1999–1995	1.118	1.833
1995–1988	0.990	1.623
1988–1983	1.135	1.862
1983–1977	1.244	2.040
1977–1967	1.121	1.839
2012–1988	0.793	1.300
1983–1967	1.208	1.981
2012–1967	0.894	1.466

Equation (2) can be used to threshold the DoD at a certain confidence limit and to attribute differences within this threshold to noise. In this study, the minimum level of detection was set with a confidence limit of 90% ( $t = 1.96$ ). For the data set used in this study, Table 2 shows the associate limits of detection.

Volumes of significant change were computed for every time step and geomorphological class for significant elevation changes at the 90% of confidence level. In order to compare landform types with different spatial extent, volumes were normalized by surface extent. To compare time periods, volumes were also normalized by the time between images. Accordingly, all results are provided in  $\text{m}^3 \text{m}^{-2} \text{yr}^{-1}$ . These statistics represent the rate of surface downwasting/deposition for each landform. If we follow *Thomas* [2001], these rates describe the sensitivity of the surface change of each landform to climate forcing, given that we can assume that all landforms have been subject to the same temperature or precipitation change. However, these are actually *absolute* measures of sensitivity as they make no reference to the magnitude of the rates of change expected under constant climate conditions, that is, the *relative* sensitivity. It is quite possible that climate forcing could cause a substantial increase in the rate of surface change for some landforms as compared with what would be expected under constant climate conditions, even though when compared with other landforms their absolute sensitivities remain small. One solution to this problem would be to calculate the change in rates of change between the periods with different climate forcing, but this characteristic is complicated by the fact that the process responses may be very different between landforms in response to climate warming and cooling. For this reason, we avoid using the term sensitivity overly in the interpretation, notably when comparing different landforms. Rather, we use the terms rates of elevation change or downwasting.

Finally, DEMs were used to orthorectify aerial imagery in ERDAS LPS. The derived orthophotos were used to estimate surface displacements using the image correlation software 7D [*Vacher et al.*, 1999]. Displacements could then be computed in pixels and converted to distances in meters. Image correlation analysis was performed for  $15 \times 15$  pixel windows. Results were filtered to eliminate erroneous matches and unrealistic displacements induced by image deformation resulting from the orthorectification process in very steep areas or cliffs where the quality of the DEMs is low. Horizontal movements were extracted as vectors of displacement at a defined window resolution. Given the 0.35 m resolution of most orthophotos, a  $15 \times 15$  pixel window corresponds to a  $5.25 \text{ m} \times 5.25 \text{ m}$  cellsize. Since horizontal displacement accounts only for XY dimensions, it is by definition an underestimation of the real displacement. Hence, outputs were divided by the cosine of the local slope to obtain the three-dimensional displacement distance. Finally, results were normalized by year in order to compare outputs obtained with imagery for different dates.

Displacement detection depends strictly on the quality and contrast of the input imagery. The latter is also dependent on the quality of the DEM, as uncertainty in elevation data can undermine the quality of the orthorectification process. Very large displacements at the surface (both vertical and horizontal deformations) may also generate decorrelation that causes the algorithm to fail to retrieve the displacement. Accordingly, not every pair of images provided results for the whole study area. To differentiate areas where information could not be derived from areas with no distinguishable displacement, a no movement and/or noise class (results inferior to 0.2 m/yr) is defined and displayed as transparent. The most complete and detailed

**Table 3.** MeteoSwiss Measurement Stations Employed

Location	Elevation (m asl)	Data <sup>a</sup>	Period	km From Arolla	Direction
GSB	2461	Temp.	1864 to present	30	Southwest
Sion	482	Temp.	1864 to present	24	North
Evolène-Villa	1826	Temp., Prec.	1987 to present	9	North
Grächen	1550	Temp., Prec.	1960 to present	34	Northeast
Hérémece	1238	Prec.	1960 to present	18	North
Zermatt	1638	Prec.	1960 to present	21	East
Bourg St-Pierre	1664	Prec.	1960 to present	23	West
Grimentz	1512	Prec.	1960 to present	19	Northeast

<sup>a</sup>Temp., temperature; Prec., precipitation.

outputs were obtained using the 1967–1977, 1977–1983, 1988–1999, and 1999–2005 pairs of imagery and are employed to investigate the response of surface displacement to climate forcing.

The interpretation of catchment-scale erosion and deposition patterns required reference to the spatial assemblage of landforms present in the study area. A geomorphological map of the region [Lambiel *et al.*, 2015] was used for this purpose and permitted derived data to be linked to specific landforms. This is crucial for the identification of the landforms most active under recent climate change and their spatial organization.

### 3.2. Data Interpretation: Climatic Context

The interpretation of mass movement in alpine environments at the decadal scale also requires reference to the climatic conditions that affected such systems. However, long-duration climatic data series are rarely available. Early climate monitoring tended to be focused on centers of population, and so climate data are often remote from many mountain study sites. In this study, the closest reliable data are available for Evolène-Villa (9 km from Arolla at an elevation of 1826 m asl), but data are available only from 1987 and so are not sufficient to characterize our period of study. Hence, it was necessary to transfer data collected from more distant locations, which may lead to uncertainties in the associated climate data because of altitude and topographic effects. Accordingly, it is important to have access to multiple data series and, if possible, under similar geographic and topographic conditions to the area of interest, to transfer them to the locality under interest and to test them on more locally available but shorter records.

In Switzerland, the Swiss National Basic Climatological Network includes 29 climatic and 46 rainfall measurement stations, some of which started in 1864. Homogenized monthly data (i.e., historic measured values adjusted to current measuring conditions) from the nineteenth century are available for 14 stations and can be used to reconstruct climatic change for the last 150 years [Meteosuisse, 2014]. To set a climate context and to sustain interpretations in the present study, data series from seven measurement stations were used (see purple dots in Figure 1 and Table 3). Two of these have long-term homogenized data: Col du Grand St-Bernard (GSB) at an altitude of 2461 m asl and 30 km to the southwest of Arolla and Sion, 482 m asl, located 24 km north. The available climatic parameters are mean annual air temperature (MAAT), annual rainfall, and snowfall and snow depth. Data are provided by the Swiss Federal Office of Meteorology and Climatology MeteoSwiss (further information and data available at [www.meteoswiss.admin.ch](http://www.meteoswiss.admin.ch)).

Long time series of snowfall and snow depth are scarce. The only data available for Arolla are daily snow depth measurements from 1998 to 2011 for Fontanesses, located at 2850 m asl above the village of Arolla (green triangle in Figure 1). Snowfall and snow depth will be strongly influenced by altitude as well as other local factors, such that relying on measurements in other sites is not optimal for reconstructing a decadal history of snowfall in the area of study. Hence, the GSM-SOCONT (Glacier and SnowMelt - SOil CONTRibution model) modeling approach developed by Schaeffli *et al.* [2005] was adopted. This is a well-established glaciohydrological model [e.g., Schaeffli and Huss, 2011; Tobin *et al.*, 2011; Godon *et al.*, 2013] which was used with available temperature and precipitation time series from proximate measurement stations (Sion and Hérémece, respectively) to extrapolate values of snow depth for elevation bands across the mountainside in Arolla. There are more complex modeling options, but these would demand additional data (e.g., measured incoming solar radiation) that are not available. The GSM-SOCONT model is detailed in Schaeffli *et al.* [2005]. The model was set to run with a daily resolution, and empirical lapse rates were employed [Bouët, 1985]. The degree-day factor for snow and the effect of elevation on precipitation were optimized using the available Fontanesses data.

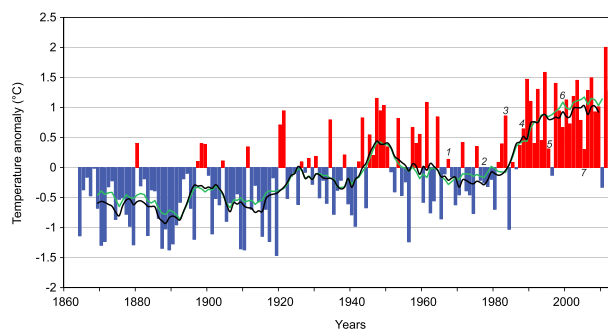


**Figure 3.** Mean annual air temperature at the Col du Grand St-Bernard between 1864 and 2013 as deviation from the reference mean established between 1961 and 1990. Trend lines indicate the 5 year moving average for that site (black) and Swiss mean (green). The numbers indicate the dates of available aerial imagery. Data: Swiss Federal Office of Meteorology and Climatology MeteoSwiss [www.meteoswiss.admin.ch](http://www.meteoswiss.admin.ch).

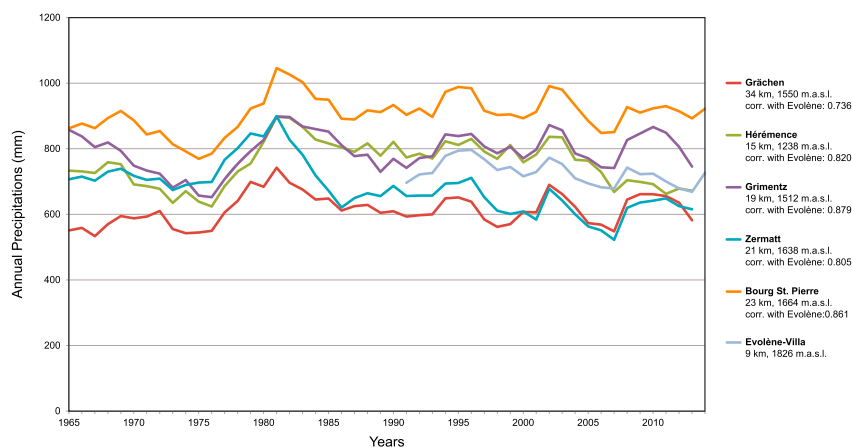
Calibration using the daily snow depth data available provided a mean error of 8.6 cm with a precision of  $\pm 38.2$  cm at the 90% confidence level, which is very satisfying given the simplicity of the model. Accordingly, the model is considered of sufficient quality to characterize the interannual snow cover trends for the site. To analyze the evolution of snow cover during the period of study, the model was used to estimate snow depth at the typical end of the accumulation period (31 March) and the typical end of the glacier ablation period (30 September) for every year from 1960 to the present at varying altitude bands but excluding the rockwalls (thus from 2100 to 2900 m asl, Figure 5a).

## 4. Results: A Quantitative History of Surface Changes in an Alpine System

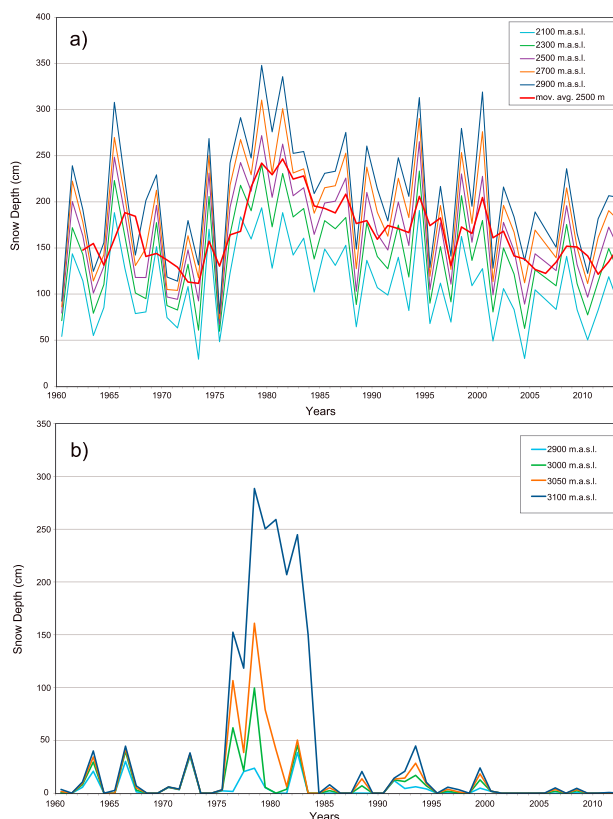
### 4.1. Climatic Evolution

Figure 3 shows the evolution of mean annual air temperature (MAAT) from 1864 to present as a deviation from the mean of the 1961 – 1990 reference period for Col du Grand St-Bernard (GSB). Comparison of the GSB 5 year moving mean with the national moving mean suggests a similar evolution of MAAT at the scale of decades. The correlation between MAAT data for Evolène-Villa and the GSB is 0.978, suggesting that the study site experienced a similar decadal-scale evolution to other regions of Switzerland. Figure 3 suggests that between the 1960s and the early 1980s there was a climatically cooler period. A very rapid warming followed from the mid-1980s to the 1990s. This trend continued, albeit more slowly, until present. With only two exceptions, the MAATs in the warming period are always higher than the reference mean, demonstrating the presence of strong temperature forcing during the last three decades.

Figure 4 presents annual rainfall data for measurement stations with similar conditions and close to Arolla. Measurements at the Col du Grand St-Bernard are not well suited for description of the Hérens valley



**Figure 4.** Annual precipitation for meteorological stations located near Arolla (5 year moving average). The legend indicates the altitude and distance for each station from Arolla, as well as the correlation 1987–2014 with Evolène-Villa precipitation. Data: Swiss Federal Office of Meteorology and Climatology MeteoSwiss [www.meteoswiss.admin.ch](http://www.meteoswiss.admin.ch).



**Figure 5.** Arolla snow depths modeled at various altitudes for (a) 31 March and (b) 30 September, using the GSM-SOCONT model. In Figure 5a, the red line represents the 3 year moving average for the 2500 m asl limit.

patterns because Grand St-Bernard is located on an alpine col on the main southern alpine drainage divide and impacted by both southern and northern rain-bearing systems. Arolla is some way north of this divide and sheltered from southerly rain-bearing systems. Instead, we focus upon comparison of Evolène with five more characteristic (altitude and geographical position) locations (Figure 4). Five year moving means are similar for the five stations. Between the end of the 1960s and the beginning of the 1970s precipitation decreased slightly before increasing considerably in the second part of the 1970s. Then, a modest decrease preceded the relative stability observed from the mid-1980s. Of particular interest are Hérémece and Evolène-Villa stations (1238 and 1826 m asl, 18 and 9 km north of Arolla, respectively), as both are located in the Hérens valley. The Hérémece data are the most complete and feature a considerable decrease in annual precipitation before a substantial increase from the mid-1970s, with a peak at the beginning of the 1980s. Afterward, precipitation was stable at around 800 mm/yr, before decreasing considerably in the 2000s. The representativeness of these data as a proxy for the Arolla case study is sustained by the strong correlation between the longer term data series and the shorter Evolène-Villa series, available from the end of the 1980s, with similar trends apparent (Figure 4).

Results produced using the GSM-SOCONT model illustrate relatively lower March snow depths in the 1960s and mid-1970s (Figure 5a). Considerable increases in snow depth are then found for the following decade, reflecting the period of greater precipitation shown in Figure 4. From 1985, end of winter snow depth appears to have decreased steadily, albeit with high variability. Snow depths at the end of the summer (Figure 5b) show how the combination of high winter snow accumulation (Figure 5a) with low temperatures translated into considerable unmelted snow at the end of the summer at the altitudes of the glacial accumulation zones for the 1977–1985 period. On the other hand, snow cover appears to completely disappear at the altitudes of interest during every summer in the 2000s. While interannual variations are very high, these results are consistent with other observations in Switzerland [Meteosuisse, 2014]. The considerable increase in snow depth observed from the mid-1970s to 1985 coincides with widespread glacial advance in the region in the early 1980s [WAV Laboratory of Hydraulics, Hydrology and Glaciology, 2013].

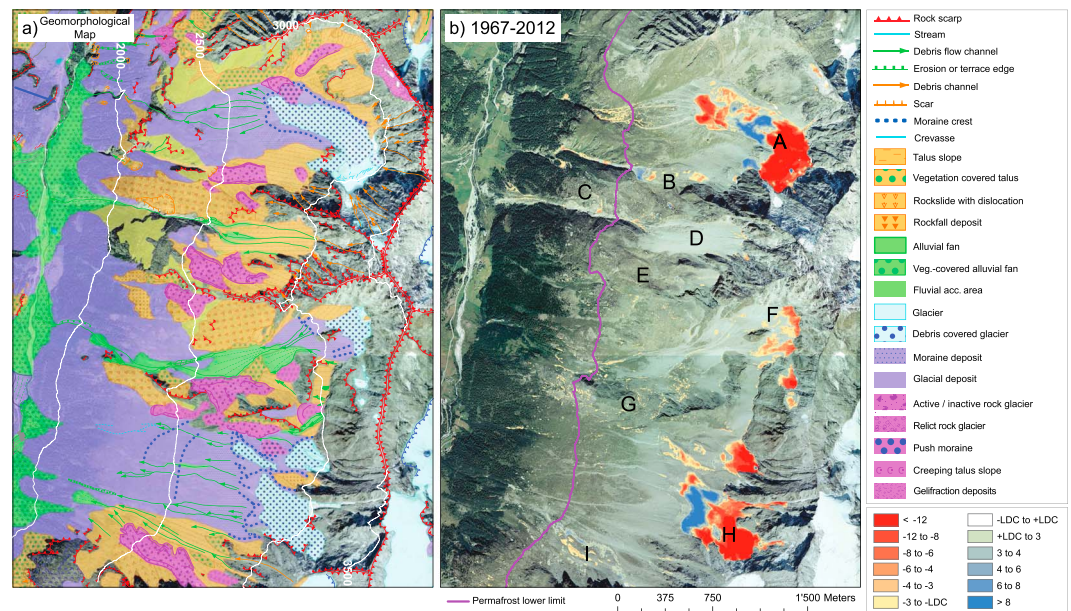


**Figure 6.** (a) Geomorphological map [Lambiel *et al.*, 2015] and (b) DEM of difference of 1967–2012, LoD 90% = 1.47 m, with regional lower limit of permafrost (~2400 m asl) [Lambiel and Reynard, 2001] and sites of interest presented in Figure 1 (orthophoto: Swisstopo 2005).

By considering the temperature, precipitation, and modeled snow cover depths together, we can consider the aerial imagery as relating to two distinct climate forcing stages: a relatively cooler and climatically more stable period (1960s to 1983) and a warming period (1983 to present). The relatively cooler and stable period is characterized by a decrease in annual rainfall at first (mid-1960s to mid-1970s) but then greater precipitation at the end of the 1970s and beginning of the 1980s. Snow cover reflected this shift, only increasing with the start of the wetter period in the second half of the 1970s and 1980s. This emphasizes the importance of interannual precipitation variability in the study site for interannual variability in snow accumulation. Precipitation decreased as the climate warmed from the early 1980s, but this trend stopped from 1990, although examples of both wetter and drier years remain. Thus, the transition to the warming period also saw a net decrease in snowfall (after the high rates of the period 1975–1983), which then stabilized until the year 2000. In the 2000s, accumulated snow in March returned to levels characteristic of the 1960s but with lower snow cover in September because of warming effects.

#### 4.2. DEMs of Difference

Figure 6a shows the geomorphological map produced by Lambiel *et al.* [2015]. The two large glacial systems of Tsarmine and La Tsa are mainly debris-covered glaciers (A and H in Figures 1 and 6b). La Tsa comprises two smaller glaciers divided by a rockfall deposit zone and a detached, small area of debris-covered dead ice. The contexts of Tsarmine and La Tsa are similar. Both sites are relatively flat, and in addition to glacier and debris-covered glacier there are also small proglacial forefields, the latter delimited by Little Ice Age (LIA) moraines. These systems are each more than 400,000 m<sup>2</sup> in area, with the glacier and debris-covered glacier parts occupying ~284,000 and 227,000 m<sup>2</sup>, respectively. The remainder of the area is mainly morainic deposits. The Genevois glacier (~65,000 m<sup>2</sup>), where ice is no longer visible, is located between these two larger glacial systems (F in Figures 1 and 6b), in a very steep location. A considerable number of active rock glaciers, mass movement processes (especially active rockslides), and fluvial process-related landforms are also mapped across the mountainside (see also Delaloye *et al.* [2007] and Barboux *et al.* [2014] for further details). Thus, the geomorphological map illustrates the presence of an assemblage of glacial, periglacial, hillslope, and fluvial landforms distributed over the area, and so a complex geomorphological setting.

Figure 6b shows the elevation changes between 1967 and 2012. Despite the substantial presence of unconsolidated material, the mountainside has been generally relatively stable at the limits of detection associated with our analysis over the last four and a half decades. Effectively, detectable surface downwasting is local. The largest magnitudes of change are found on glaciers and debris-covered glaciers. In the upper part of the

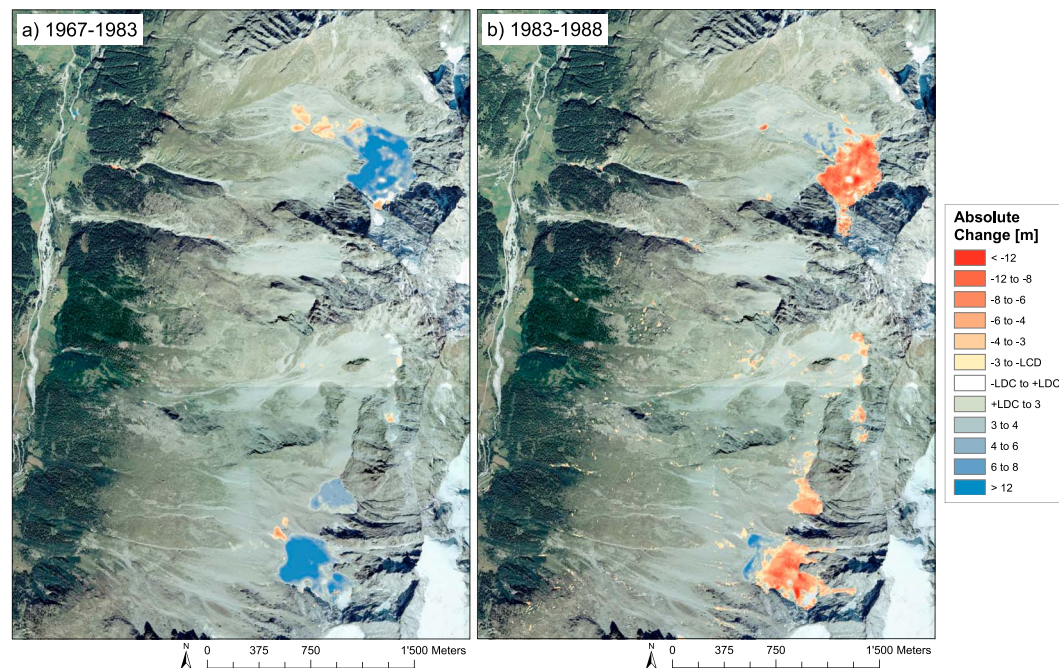


**Figure 7.** (a) DEM of difference of cooler and stable temperature period, 1967–1983, LoD 90% = 1.98 m and (b) DEM of difference of rapid warming period, 1983–1988, LoD 90% = 1.86 m (orthophoto: Swisstopo 2005).

Tsarmine and La Tsa systems, vertical loss is generally greater than 12 m, with peaks of more than 20 m. In their middle parts, increases in elevation of between 10 and 20 m are observed. It is probable that ice loss in the central part of these systems was mitigated by thickening caused by ice flux from upstream, with a possible legacy from glacier growth in the 1960s–1980s (see below). In Tsarmine, the lower part of the glacier suggests considerable downwasting. This is somewhat more limited in the Tsa system. In both cases, it suggests zones of elevation loss due to glacier marginal ablation. The Genevois glacier experienced only elevation loss and in reduced proportions as compared with the other glacier systems, a fact that could be explained by its smaller size.

Only the activity of two rock glaciers is clearly identifiable in the DEMs of difference: the Tsarmine rock glacier, located southwest of Tsarmine glacier (B in Figures 1 and 6b), and La Roussette, the most southern of all the area of study (I in Figures 1 and 6b). For both rock glaciers, an advancing front is evident, confirmed by an increase in elevation in their lower parts. The other rock glaciers in the mountainside show very little substantial downwasting over the 45 year period considered here. However, to conclude that these landforms are less active or inactive, it is also necessary to consider horizontal displacements especially as there may be lateral fluxes without elevation changes or ones that cannot be detected by the DoDs given their precision.

Gravity-related processes have vertical changes of a magnitude smaller than glacial and periglacial landforms. Nevertheless, rockslide activity produced significant downwasting in some locations over the 45 years considered. The most evident example is the Perroc rockslide located next to the Tsarmine rock glacier (C in Figures 1 and 6b), with traces of sliding toward the debris flow channel that connects the Perroc talus slope (D in Figures 1 and 6b) to the valley bottom. Traces of rockslide activity, although less marked, are also visible for the rockslide situated west of the La Tsa hut (G in Figures 1 and 6b). Detectable elevation changes were not encountered in talus slopes. Erosion and deposition on the mountainside by fluvial processes also appear to be limited given the precision of our data. Channel excavation is limited to a few cases. Notably, it can be seen in the debris flow channels beneath Tsarmine, at the top and at the base of the Perroc talus slope, and in the debris flow channels extending from the Genevois glacier toward the valley bottom.

Figure 7 compares the DoDs for two distinct climatic periods: the cooler period that ended with some snow accumulation (a) and a rapid warming period (b). A distinct landscape response is shown for both periods. The mountainside appears to be very stable during the cooler period; the only significant elevation changes are associated with the glaciers with gains of several meters. Downwasting is very low and visible only in a

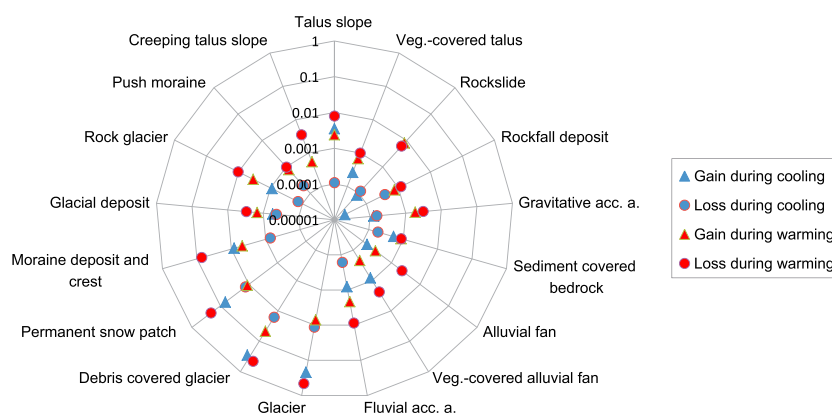


**Figure 8.** Average yearly volumetric changes for cool/stable and warming periods for different landforms, normalized by their spatial extent ( $\text{m}^3 \text{m}^{-2} \text{yr}^{-1}$ ). An absent symbol means no change.

few patches especially on the lower part of the Tarmine and La Tsa glacier systems (A and H in Figure 1). The patterns observed during the rapid warming period of the 1980s are in the opposite direction. The glaciers experienced a loss in elevation of 4 to 10 m in their upper part. The elevation gain in their middle part, already visible in Figure 6b, is observed here but is of lower magnitude (3 to 6 m) and of smaller extent. More isolated but significant elevation changes, which were completely absent during the cooler period, are found across the hillslope. These changes relate mostly to gully erosion on terminal moraines, shallow excavation of debris flow channels, slight signs of activity at rock glacier fronts, or rockslide activity.

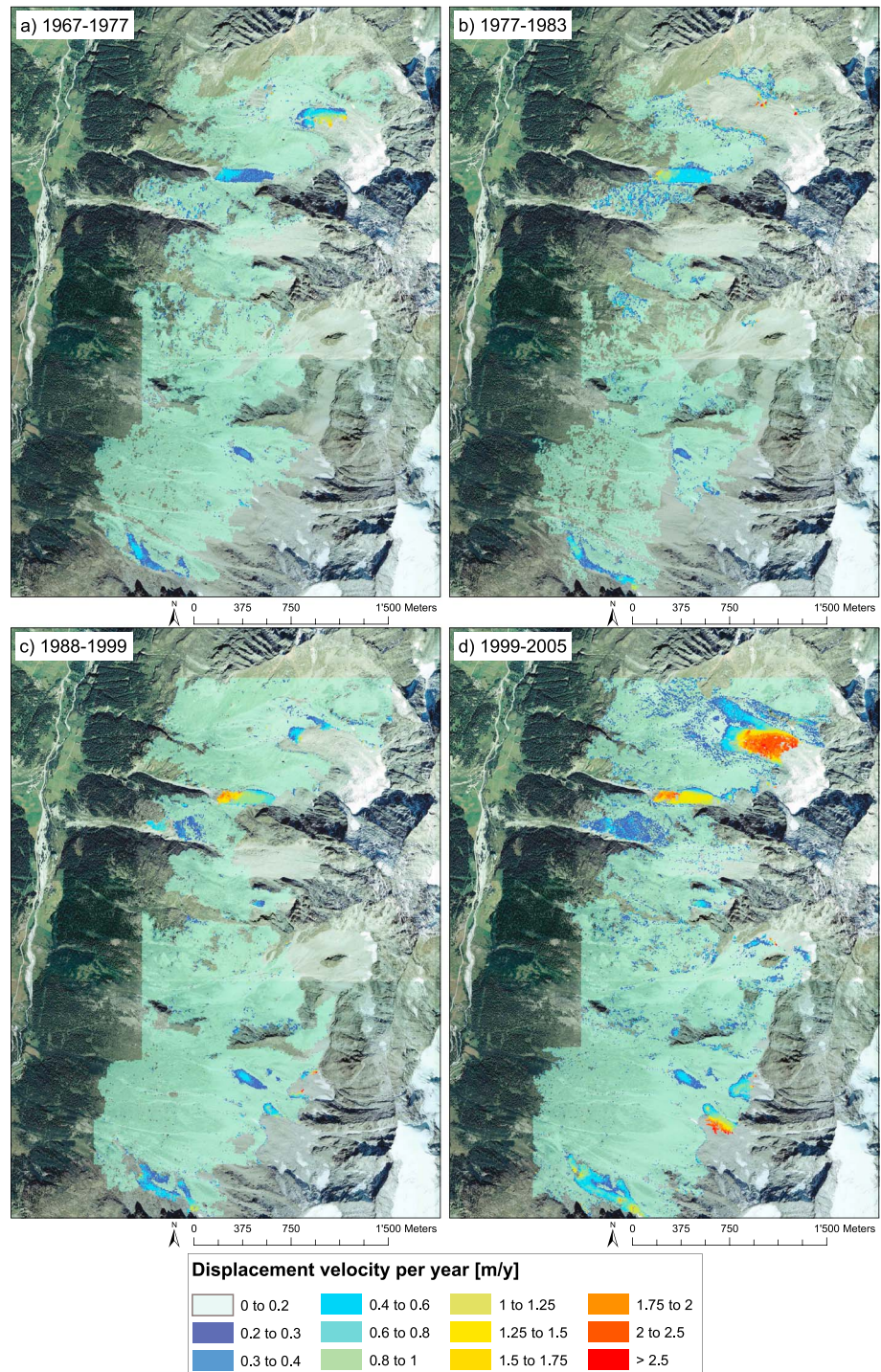
#### 4.3. Rates of Surface Change

Figure 8 shows average volumetric rates of surface change (in  $\text{m}^3 \text{m}^{-2} \text{yr}^{-1}$ ) for cooling/stable (blue symbols) and warming periods (red symbols) for every landform on the mountainside. This helps to better identify the dominant pattern for every landform type and link each to the effects of climate forcing. First, rates of change for parts of the landscape associated with glacial processes (i.e., glacier, debris-covered glaciers, moraine deposits) are logically greater than for other landforms, a fact already visible in the DoD (Figures 6b and 7). Glacial landforms have the greatest rates of gain during colder periods, while their rates of loss under warming are the greatest changes observed. Second, some landforms have enhanced activity during the warming period. Examples are rock glaciers, talus slopes, and rockslides. For these landforms, both rates of gain and loss during warming are greater than changes in the cooler period. Third, for many landforms, rates of gain are greater than losses in the climatically cooler and stable period. Afterward the opposite is observed, with rates of loss becoming considerably larger than rates of gain during the warming that started in the mid-1980s. The clearest examples are talus slopes, rockslides, alluvial fans, moraines, and rock glaciers. Finally, average rates of loss per year during the warming period are comparable to rates of gain during the cooling stage for debris-covered glaciers ( $0.33$  and  $0.31 \text{ m}^3 \text{m}^{-2} \text{yr}^{-1}$ , respectively) but differ for bare ice glaciers ( $0.46$  and  $0.21 \text{ m}^3 \text{m}^{-2} \text{yr}^{-1}$ ). Debris-cover glaciers also have higher rates of volumetric gain during warming than loss during cooling, but this appears to be mostly a product of mass displacement rather than cryogenesis or sediment supply.

#### 4.4. Surface Displacements and Deformations

Figure 9 shows the norms of displacement vectors (horizontal vectors corrected for slope) normalized by number of years for four distinct image pairs. It should be noted how some very active areas such as glaciers and debris-covered glaciers are not highlighted despite being the areas where most consistent movements are expected. This is for two reasons: first, vertical changes in these areas are very high (see Figures 6b and 7), and thus surface changes are so great that the resulting decorrelation prevents the detection of movement using image correlation analysis. Second, these areas are also likely to feature less ideal contrast because of their snow or ice cover. This is particularly true for the 1977 imagery as the mountainside is partially snow-covered in its upper part.

The surface displacements mapped between 1967 and 1977 (Figure 9a) highlight areas where significant elevation changes were not identified by the DoD (see Figure 7a). Rock glacier activity is evident with movements of up to  $0.6 \text{ m/yr}$  for the Tarmine and La Roussette rock glaciers (B and I in Figures 1 and 6b) but



**Figure 9.** Norm of displacement vectors per year for (a) 1967–1977, (b) 1977–1983, (c) 1988–1999, and (d) 1999–2005 (no data: displacement information not available, orthophoto: Swisstopo 2005).

absent or less well defined for others. The large Perroc rockslide (C in Figures 1 and 6b) also features localized displacements that can reach 0.3–0.4 m/yr. Even though only the lower parts of the glacial and proglacial systems were visible, probable ice-related movements can be identified. In particular, velocities up to 1.75 m/yr are identified in Tsarmine (A in Figures 1 and 6b). From the period 1977 to 1983 (Figure 9b), the snow cover of the 1977 images, along with the low quality of those of 1983, lead to large data gaps (especially in the northern part of the image) with many scattered, noisy displacements. Nonetheless, creep of the Tsarmine

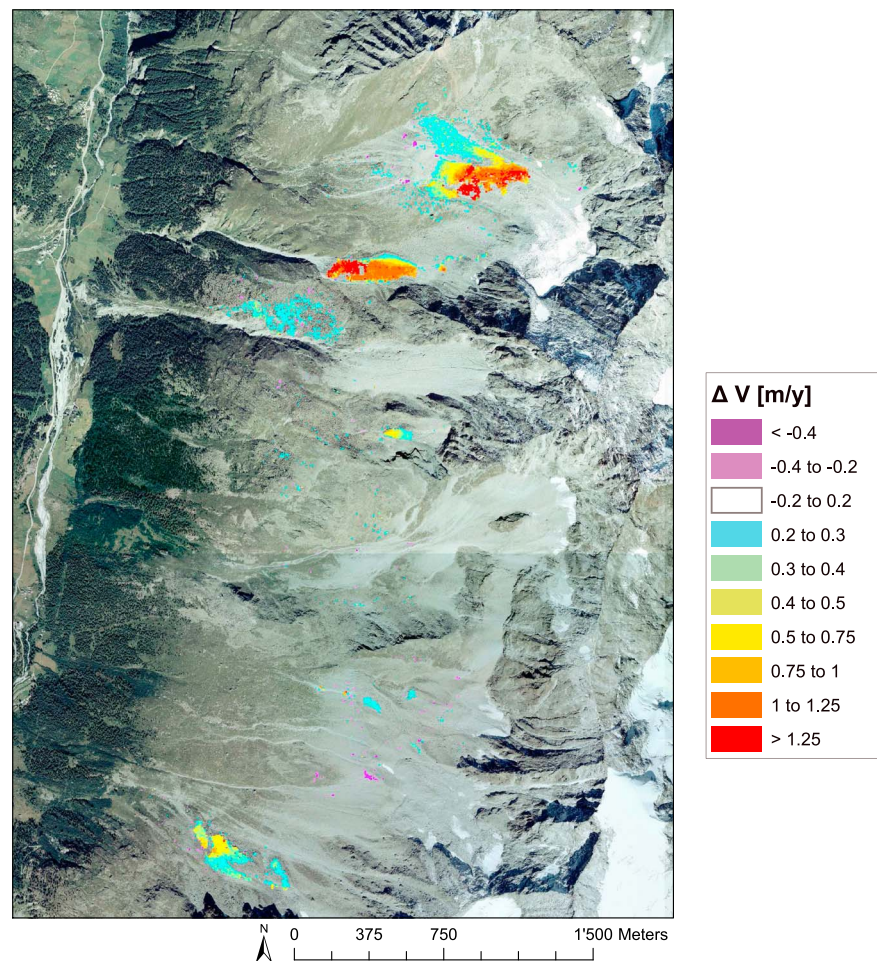


**Figure 10.** Differences of the norm of displacement vectors between 1967–1977 and 1999–2005: positive values indicate acceleration (orthophoto: Swisstopo 2005).

and La Roussette rock glaciers could be identified with a slight acceleration. The large rockslide mentioned earlier appears more active than the previous epoch.

An enhancement of periglacial activity seems to occur between 1988 and 1999 (Figure 9c). The Tsarmine rock glacier experienced an acceleration with velocities of up to 0.75–1 m/yr in its upper part and up to 2 m/yr near its front. La Roussette rock glacier also experienced a slight acceleration and has velocities of  $\sim 0.5$ –0.75 m/yr. Displacements on other rock glaciers are also increased and hence now visible. The rock glacier located between the Perroc talus slope and the Genevois basins, west of Dent de Perroc (upper part of the rock glacier called Lé Bláva, E in Figures 1 and 6b), which appeared stable in terms of elevation changes, reached velocities of  $\sim 0.4$  m/yr. Movements on the large rockslide are not considerably enhanced with respect to the colder period.

The analysis of displacements between 1999 and 2005 (Figure 9d) provides more complete results. Generally, greater displacement velocities than previous epochs are evident. The Tsarmine and La Roussette rock glaciers (B and I in Figures 1 and 6b) have increased velocities, up to more than 2 and 1.2 m/yr, respectively, while the rock glacier between Perroc and Genevois reached a velocity of more than 0.7 m/yr at its front. The large Perroc rockslide (C in Figures 1 and 6b) has a more homogeneous displacement. Its velocity is of the order of  $\sim 0.25$ –0.3 and 0.4 m/yr in its upper and lower parts, respectively. In the lower part, a detachment niche is well identified; it delimits a zone characterized by slightly faster displacements. Movements of debris-covered glacier systems are better highlighted and have high displacement velocities that can reach more than 2.5 m/yr in the middle part of these systems. In Tsarmine (A in Figures 1 and 6b), the velocities of the push

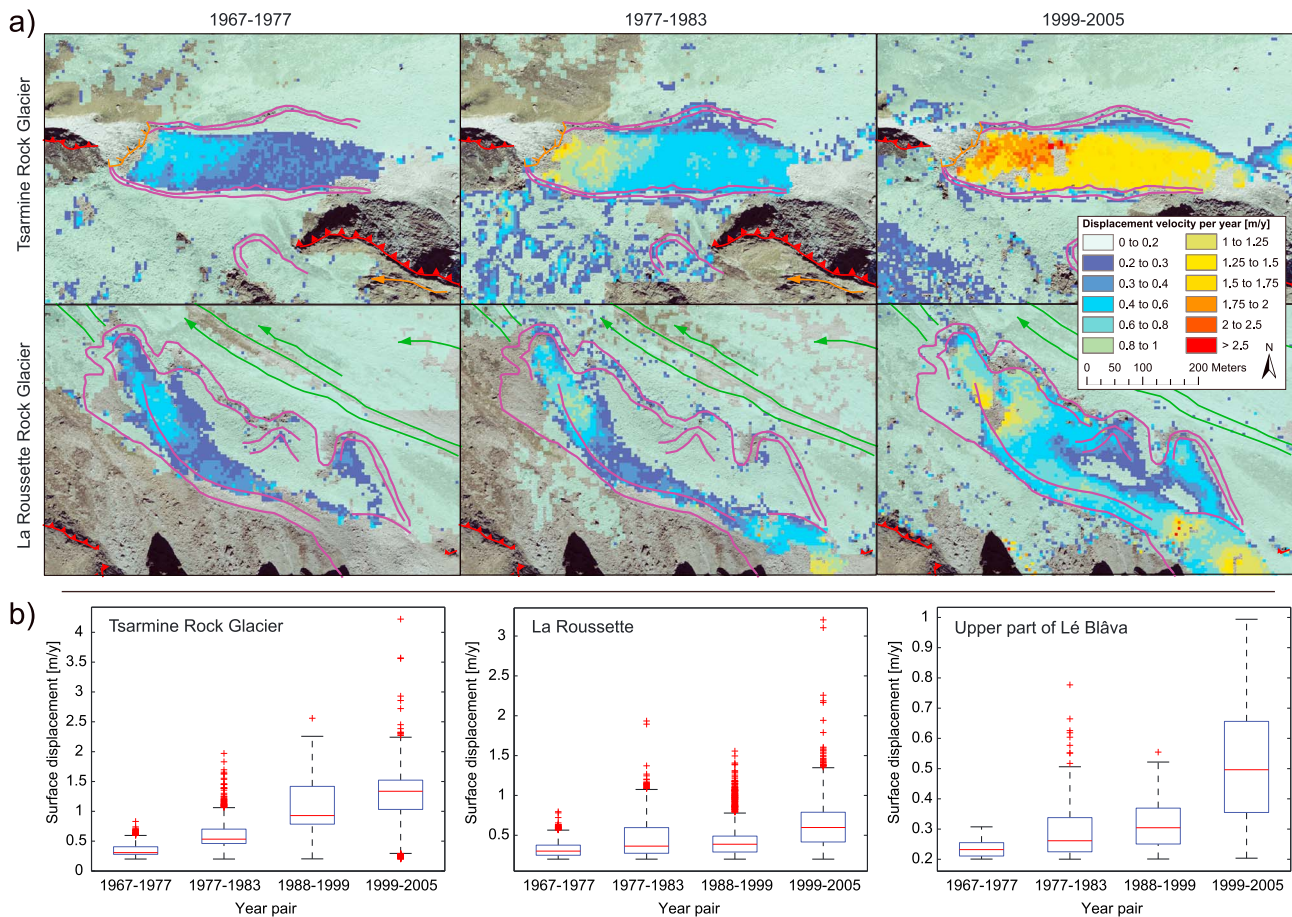


**Figure 11.** (a) Detail of displacement velocities for the Tsarmine and the La Roussette rock glaciers (orthophoto: Swisstopo 2005). (b) Boxplots of rock glacier surface velocities (Note the different scale of the vertical axes).

moraine and of the marginal rock glacier are much slower (below 1 m/yr). The same is true for the dead ice in the lower part of La Tsja proglacial forefield (H in Figures 1 and 6b).

Differencing the norm of the displacement vectors between cold and warm period, represented here by 1967–1977 and 1999–2005 pairs, highlights changes in velocities (Figure 10) that are measures of land surface acceleration/deceleration. There is discernible acceleration of the Tsarmine rock glacier (B in Figures 1 and 6b), where the increase in horizontal velocities reaches 1.5 m/yr (200 to 350% of velocity enhancement). This trend is also important for other rock glaciers; despite incomplete information, the Roussette rock glacier body (I in Figures 1 and 6b) does not seem to have experienced velocities above 0.8 m/yr (acceleration of 50%), yet in its lower part local peaks with more than a 300% increase in velocity can be observed. The west Perroc reactivation is reflected in a velocity increase of 0.8 m/yr. The same is true for the rock glacier at the margin of the Tsarmine glacier (A in Figures 1 and 6b), which reactivated and experienced a velocity increase of 0.3–0.4 m/yr. The Perroc rockslide (C in Figures 1 and 6b) is very active and experienced velocity increases of the order of 0.2–0.3 m/yr. Between 1999 and 2005, higher displacement velocities were also observed on debris-covered glacier surfaces, where for the identifiable velocity increases can reach 1.5 m/yr (acceleration of 100%). In the lower part of these systems, increments in velocities are limited to 0.2–0.4 m/yr. Decelerations are identified only very locally. The most evident clusters are concentrated on the moraine bastions of Tsarmine and La Tsja glaciers. These decreases in mass movement speed seem more related to single events of gullyng or gravitational sliding that occurred during the 1960s and 1970s than a continual process.

Figure 11 shows a more detailed view of displacement velocities for the Tsarmine and La Roussette rock glaciers (a) and boxplots of velocities for the three most active rock glaciers in the study area (b). As visible in previous images, these show different velocities under the influence of local conditions. Nonetheless, their median displacements were very similar between 1967 and 1977: 0.23, 0.30, and 0.31 m/yr for the lobe

above Lé Blâva, La Roussette, and Tsarmine rock glacier, respectively (B, above E and I in Figures 1 and 6b). Afterward, despite large velocity differences, the Tsarmine rock glacier and the rock glacier lobe above Lé Blâva have a clear increase in their velocities through time (Figure 11b). Median movements for these rock glaciers between 1999 and 2005 are 1.34 and 0.5 m/yr, respectively, corresponding to accelerations of 432% and 217% with respect to the first, cooler period. Acceleration of the La Roussette rock glacier is less evident in the velocity data illustrated in Figure 11b, despite it being visible clearly in Figure 10. Nevertheless, an increasing trend is still visible and certified by the doubling of median displacement velocities (from 0.3 to 0.6 m/yr) and by the faster outliers occurring between 1967 and 2005.

## 5. Discussion and Interpretation

The analysis of elevation changes between 1967 and 2012 (Figure 6b) highlights a general stability of this steep hillslope, and this despite the presence of unconsolidated materials. Nonetheless, warming periods seem to be associated with some detectable increases in both downwasting and surface displacement, something that has been observed in studies of similar environments [Huggel *et al.*, 2010, 2012; Beylich *et al.*, 2002; Fischer *et al.*, 2012]. The most dynamic periods are associated with either or both higher rainfall and snowfall or greater temperatures. The greatest rates of change are spatially delimited and concern mostly glacial and periglacial landforms.

### 5.1. Glacial Systems

Surface change during the relatively cold period (1967–1983, Figure 7a) shows several meters of elevation gains in the upper parts of glacial zones. This growth in the accumulation area is most likely to be cryogenic. The period 1967–1983 effectively featured favorable climatic conditions for glacial advance. Low temperatures and abundant precipitation and snow cover, from the mid-1970s, possibly translated into larger amounts of unmelted snow at the end of the warm seasons (Figure 5b) and hence in glacier growth. Conversely, high-magnitude downwasting occurred in the same areas during the warming period that begins in the 1980s (Figure 7b). This period is characterized by a rapid temperature rise (Figure 3) and reduced precipitation and lower snow cover (Figure 5a). The changes identified demonstrate distinct response to warm and cold periods and to changes in precipitation, an observation confirmed also by volumetric trends (Figure 8) especially, but not exclusively, for glaciers and debris-covered glaciers.

The 1967–2012 DoD highlights a dominance of the warming climate conditions compared to the cooler period in the form of the extensive loss of ice volume. This is caused by the longer duration of the warming period, but for the bare ice parts of glaciers it is also a consequence of the difference in average volumetric changes between gain during cooling and loss during warming ( $0.21$  and  $0.46 \text{ m}^3 \text{ m}^{-2} \text{ yr}^{-1}$ , respectively, Figure 8). For debris-covered glaciers, these rates are almost the same ( $0.31$  and  $0.33 \text{ m}^3 \text{ m}^{-2} \text{ yr}^{-1}$ ), a fact that can be attributed to the low thermal conductivity of debris covers [Takeuchi *et al.*, 2000; Lambrecht *et al.*, 2011] and to an underestimation of the melting rate during the warming period caused by the effect of ice flux from the accumulation area. Nevertheless, debris-covered glaciers also shrink considerably (see Figure 6b), and so the periods 1967 to 1983 and 1983 to 2012 represent climatic conditions either side of a critical threshold (or equilibrium state [Phillips, 2009]) for the altitude and aspect of this mountainside. The continuous glacier shrinkage from 1983 to 2012 occurred despite snow cover that was greater than the 1960s. This slight increase was not sufficient to compensate the temperature rise in these systems. Increases in elevation observed by debris-covered glaciers despite this warming are believed to be caused by the complicating effect of ice flux from the accumulation area rather than a changing pattern in the climate forcing reaction.

The case of Tsarmine (A in Figures 1 and 6b) is particularly interesting because of its heterogeneity and complexity [Lambiel *et al.*, 2004]. In the geomorphological map (Figure 6a) the following land surface types are identifiable: bare ice glacier, debris-covered glacier, push moraine, rock glacier, and moraine crests or deposits. Bare ice glaciers experienced cryogenesis (formation of ice from unmelted snow at the end of the warm season) during the 1960s and 1970s and ice ablation afterward, starting from the mid-1980s. Even though surface velocities could not be derived for this area, it could be hypothesized that ice flow is relevant and sufficient to supply ice to the middle part of the system. Effectively, the debris-covered glacial part of the system suggests that it is supplied by ice and sediment produced by rockwalls that are sufficient to counter ice melt. The debris-covered glacier has a high surface velocity (up to 2.5 m/yr). Distinctions between stable and warming periods can also be made: while both periods feature a flux, there is a surface increase between the two periods (Figure 10), of up to 1.5 m/yr. The push moraine and rock glacier are distinguished in the

geomorphological map, but this ice-debris mixture area has homogeneous patterns. Significant vertical changes are only visible at long timescales, and rates of downwasting are among the lowest of the Tsarminne system. Substantial surface displacements could not be detected during the cold period, while velocities of 0.3–0.4 m/yr were estimated during the warming period. These velocities are close to those estimated by *Kneisel and Kääh* [2007] between the 1980s and the mid-1990s (thus the first part of the warming period) for a similar context also in the Swiss Alps. Accordingly, this area seems to accelerate its creep under the influence of warmer conditions. Finally, moraine deposits appear relatively stable from a displacement point of view. In summary, the Tsarminne area is a very active system featuring a coexistence of glacial and periglacial dynamics (i.e., push moraine and rock glacier) but with constant glacial recession over the last three decades.

### 5.2. Rock Glaciers

The rates of activity that are visible in the DoDs also can vary within classes of landscape elements. As mentioned in the previous section this is the case for rock glaciers. Only the Tsarminne and La Roussette rock glaciers (B and I in Figure 1) have identifiable elevation changes between 1967 and 2012 (Figure 6b). These rock glaciers appear to be among the most active parts of the hillslope, and a possible explanation would be a combination of local topographic and subsurface ice conditions [*Lambiel et al.*, 2004; *Barboux et al.*, 2014]. Detectable elevation changes during the last decades (Figure 6b) are not homogeneous and of the order of 0.1 m of vertical change per year as observed by *Kääh* [2002] for a rock glacier in the eastern Swiss Alps. Despite the relatively small magnitude of vertical changes in the DoDs (Figure 6b), volume estimations highlight an enhanced activity from the 1960s to present. Both yearly rates of gain and loss during the warming period are higher than the values estimated for the cooling period (Figure 8), indicating a clear reaction to a warmer climate.

More interestingly, evaluation of surface displacement shows an acceleration of rock glaciers from 1967 onward. Speedup between the periods 1967–1977 and 1977–1983 may be linked with enhanced precipitation and the greater snow cover (Figures 4 and 5) that could have caused water infiltration and accelerated creep [*Ikeda et al.*, 2008]. In addition, snow conditions exert a dominant role on ground temperatures by insulating the ground surfaces from the atmosphere during winter [*Keller and Gubler*, 1993]. Early winter snow falls, coupled with a thick snow cover and late melt, may provoke an increase of mean annual ground surface temperature and rock glacier acceleration [*Delaloye et al.*, 2010; *PERMOS*, 2013]. The high snow depths of the period 1977–1985 may thus have been responsible for the observed increases in rock glacier velocities. Velocities increased even further after the transition into the warming period. The Tsarminne rock glacier velocities increased from 0.3 to more than 2 m/yr. The very high velocities of recent decades have also been confirmed by differential GPS (dGPS) measurements [*Delaloye et al.*, 2008; *PERMOS*, 2013] and InSAR data [*Lambiel et al.*, 2008; *Barboux et al.*, 2014]. The trend is the same for La Roussette, where velocities of 0.2–0.5 m/yr (comparable with other studies in Switzerland [*Kääh*, 2002; *Delaloye et al.*, 2008]) increased to 1.2 m/yr during the warming period.

The velocities of rock glaciers that were otherwise unchanged in terms of detectable elevation changes could also be observed, as for the small rock glacier located above Lé Bláva (E in Figure 1), between the Perrot talus slope and the Genevois basins. Its activity is much reduced in respect to the previous examples, and it appeared to be inactive between 1967 and 1977. Despite temperatures still being low, modest displacement is identified at its front between 1977 and 1983, probably due to the input of water caused by enhanced precipitations and melting snow. It experienced a complete reactivation during the warming period with surface velocities up to more than 0.8 m/yr. Another rock glacier located only 500 m west from it is not experiencing the same reactivation. Hence, local conditions appear to exert an important impact upon rock glacier response to cooling and warming [*Kirkbride and Brazier*, 1995]. However, some rock glaciers did accelerate first under the influence of important water inputs toward the end of the cooler and stable period (1977–1983) and then (1988 onward) under the influence of temperature rise (see Figure 11). This supports the hypothesis of a strong influence of climate forcing upon rock glacier velocities [e.g., *Kellerer-Pirklbauer and Kaufmann*, 2012], which has also been demonstrated in other studies [*Roer et al.*, 2005, 2008; *Kääh et al.*, 2007; *Delaloye et al.*, 2010].

### 5.3. Gravity-Driven and Fluvial Processes

Activity associated with gravity-driven and fluvial landforms in the DoDs is less clear than for glacial and periglacial landforms, because of the smaller magnitude of elevation changes in these areas. With the available resolution of the data and the consequent limits of detection, the activity of some small-scale geomorphic processes cannot be measured. Clear examples are rockfall activity (impossible to observe because

of the steepness of rockwalls) and debris flows of small to moderate magnitude. This leads to an underestimation of possible sediment fluxes in the system and, unfortunately, a limit of the use of the archival imagery in this study. Nevertheless, despite leaving weaker signals in the DoDs than ice-related landforms, the analysis of gravitational processes still shows changing patterns through time. In Figure 8, the rates of change during the warming period appear generally greater than in the cold period. This is clearly the case for rockslides, where both rates of aggradation and degradation appear to be considerably higher than in the cooler period. Given the location of large rockslides above the lower permafrost limit, a speculative explanation could be related to the presence of permafrost. This hypothesis requires in situ measurements to be confirmed, which are not available at present. The only case of surface displacement change between the 1960s and the 2000s is in terms of the large Perroc rockslide (C), where accelerations of between 0.2 and 0.5 m/yr are observed [Figure 10, also detected using InSAR data by *Delaloye et al.*, 2007]. The rockslide started accelerating in the cold period, probably due to enhanced rainfall and snowmelt input enhancement at the end of the 1970s. Despite less clear signals, it appears that even non-ice-related landforms might respond to climate forcing and accelerate under wetter and warmer climatic conditions, a consideration supported by similar studies [*Huggel et al.*, 2010, 2012; *Bennett et al.*, 2013].

#### 5.4. Impacts on Sediment Flux at Landscape Scale

Some landforms are found to be sensitive to warming or snow cover and rainfall increases and may lead to locally high sediment flux. Nevertheless, there is evidence in our analysis to suggest that the effects of past climatic conditions upon the landscape has left a heritage in the system that can play a key role in disconnecting zones of high rates of change from the valley bottom. The role of hillslope coupling within the fluvial and torrential systems commonly responsible for sediment transmission downstream has been widely investigated. Various studies [e.g., *Heckmann and Schwanghard*, 2013; *Harvey*, 2002] have demonstrated that in most cases only a small percentage of the hillslope is coupled to the channel network because of natural or anthropogenic barriers, leading to abundant hillslope sediment storage. In such cases, the effects of changes in erosion and deposition may be spatially restricted [*Harvey*, 2001]. Figure 12 illustrates the northern part of the study area, where examples of different connectivity settings are found. The Tsarmine glacial system (Figure 12, site 1—A in Figure 1), which is showing considerable surface change both vertically and horizontally (see Figures 6b and 9) and likely being supplied by sediments from the rockwalls located above it, is in a disconnected setting. Effectively, the depression behind the LIA moraine crest prevents sediment transfer down the mountainside despite the large availability of unconsolidated material in the site. Sediment transfer may occur from gully erosion on the moraine bastion, as testified by the presence of debris flow channels. However, recent sediment delivery to the valley bottom is not observed, and associated alluvial fan dynamics are very limited or even absent (Figure 12, AF1). This type of disconnection, associated with high sediment availability, is also found for the La Tsa glacier system.

The second state observed is intermediate storage as in the case of the Tsarmine rock glacier (Figure 12, site 2—B in Figures 1 and 6b). Rock glaciers act as sediment buffers on the hillslope. The role of permafrost is essential in this regard, as ground ice is able to prevent or block the mobilization of unconsolidated sediment. Rock glacier acceleration under warming or wetter climatic conditions could translate into shorter intermediate storage of material. Effectively, the increased velocities of the Tsarmine rock glacier should eventually translate into more sediment delivery to the channel downslope. However, the large boulders delivered to the front of the rock glacier are deposited into a narrow channel with relatively limited water supply and so transport capacity. Extensive boulder deposits are found in the channel, but they do not propagate to the valley bottom. As a result, the alluvial fan below does not receive the sediment supply that is expected given the velocity of the rock glacier (Figure 12, AF2). Despite evidence of enhancement of sediment production at the rock glacier front, it can be hypothesized that delivery at the valley bottom may not be strongly affected by climate forcing at the timescales considered. The condition of the La Roussette rock glacier is different: here the disconnection is caused by the fact that its front does not deliver sediments to a channel. It acts as a sediment sink for the wide mountainside topography to its south and effectively insulates any possible upstream increase in sediment flux from propagation through to a channelized system and hence the valley bottom.

Finally, the Perroc talus slope (Figure 12, site 3—D in Figures 1 and 6b) appears to be characterized by a good, efficient connection. Effectively, the intermediate storage here is the talus slope itself, in a very steep condition that facilitates sediment mobilization by debris flows starting in the overhanging rock couloirs. As a consequence, sediments from rockwalls, the talus slope, and even landslides at the edges of the Perroc rockslide are easily transferred through the channel, aided by a linear, steep, and buffer-free connection.

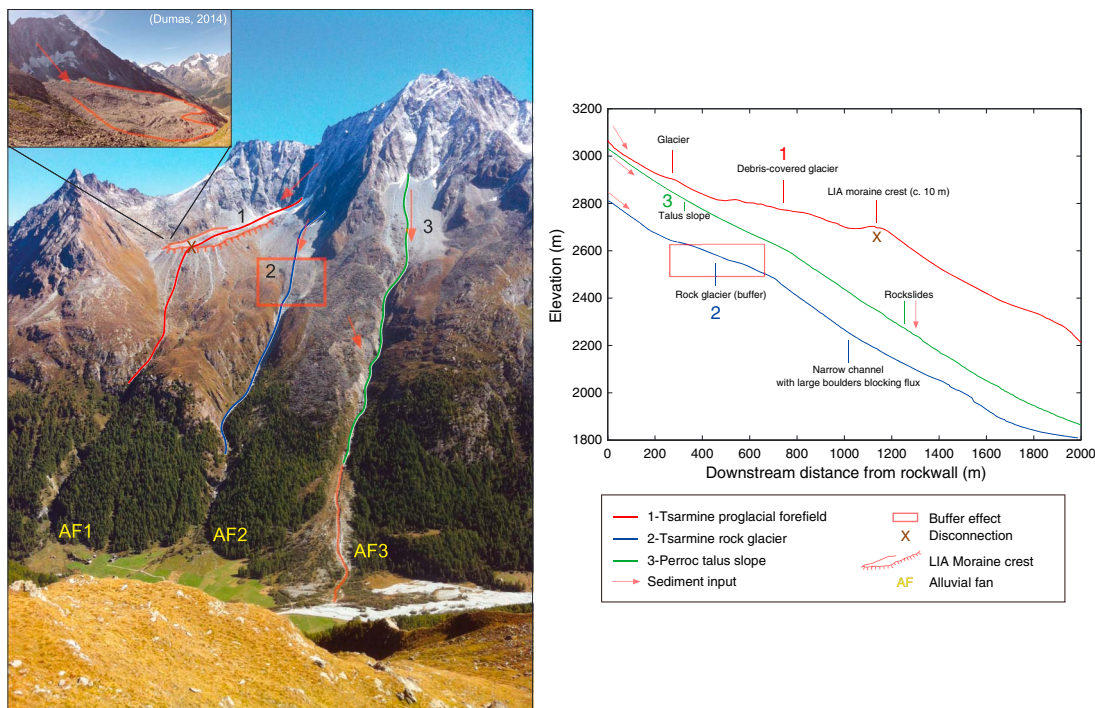


**Figure 12.** Different connectivity settings in the northern part of the mountainside: disconnection of the Tсарmine glacial system (1), intermediate storage and buffering of the Tсарmine rock glacier (2), and established connectivity of the Perroc talus slope (3). In the lower part it is possible to observe the contrasting conditions of alluvial fans caused by different sediment connectivity.

Thus, the largest and apparently most active alluvial fan (Satarma, Figure 12, AF3) is associated with the best sediment connectivity and not with large surface changes upslope or the largest sediment availability. Thus, connectivity plays a key role in climatically driven sediment dynamics, an observation that finds support in other contributions [Shroder *et al.*, 2000; Harvey, 2001; Reynard *et al.*, 2012; Bosson *et al.*, 2014]. In another Swiss case study, Müller *et al.* [2014] noted that the actual mobilized material at the top of the sediment cascade is much higher than the input in the subsystems throughout the hillslope. Geilhausen *et al.* [2013] observed that while climate change and enhanced glacier retreat led to an increase in sediment discharge from proglacial zones, downstream sediment fluxes were considerably reduced by the development of proglacial lakes. Accordingly, intermediate storage of loose material exerts a critical control on climate forcing signals in alpine systems [Matsuoka, 2008]. This leads to the counterintuitive observation that while landscape response to climatic warming and enhancement in precipitation and snow cover implies a net increase in sediment flux toward the valley bottom, this is not necessarily manifest in the valley bottom itself (e.g., in evident increase in alluvial fan dynamics) because this flux is commonly disconnected for the most reactive parts of the landscape. This is particularly true for small glacier systems, where the rate of paraglacial activity is high but glacier erosion and the geometry of past deposits prevent sediment flux downstream [e.g., Brazier *et al.*, 1998; Shroder *et al.*, 2000; Benn *et al.*, 2012; Bosson *et al.*, 2014]. As Ballantyne [2002] argues, paraglacial system sediment release may be delayed to centuries or even millennia after the beginning of deglaciation. Reflecting wider observations of hillslope buffering of catchment response to external forcing [e.g., Forzoni *et al.*, 2014], it questions the extent to which decadal-scale, perhaps even centennial-scale, climate forcing can be quantified in valley bottom (e.g., lake) deposits in mountain environments.

## 6. Conclusion

By unlocking the information held in archival aerial imagery, this contribution has been able to associate changes in climate forcing to modifications of alpine geomorphic processes and rates. This was manifest as a distinct landscape response to warm and cold periods and to changes in rates of precipitation and snow cover. From the end of the 1960s to the beginning of the 1980s, despite temperatures still being warmer than during the Little Ice Age, glaciers were able to grow substantially at rates of  $\sim 0.3 \text{ m}^3 \text{ m}^{-2} \text{ yr}^{-1}$ ,

while widespread stability was observed for other landforms. The reaction to the rapid warming that followed was fast and seemed to pass a threshold, with a continuous glacial shrinkage observed from the mid-1980s. Estimated melt rates for bare ice glaciers are higher than for their debris-covered parts ( $0.46$  versus  $0.33 \text{ m}^3 \text{ m}^{-2} \text{ yr}^{-1}$ ), because of the insulating role of debris [Takeuchi et al., 2000; Lambrecht et al., 2011] and the effect of ice flux from the accumulation zones to the debris-covered parts of the systems. Precipitation and snow cover considerably increased from the mid-1970s and, despite stable and low temperatures, were associated with a general acceleration of surface displacements for different landforms, especially rock glaciers. Moreover, the continuation and accentuation of temperature rise translated into an augmentation of these displacement velocities. Active rock glaciers experienced velocity increases from  $0.2$ – $0.3 \text{ m/yr}$  to more than  $1 \text{ m/yr}$  during the period of study, with peaks as high as  $2 \text{ m/yr}$ . A reactivation of an inactive rock glacier has also been observed. Non-ice-related landforms also appear to accelerate their displacements under wetter and warmer climatic conditions; the most evident examples are velocity increases of between  $0.2$  and  $0.5 \text{ m/yr}$  for a rockslide. Despite some landforms being able to generate an enhanced sediment flux locally, propagation throughout the hillslope is not a direct consequence because of disconnection. Hence, the consequences of climate forcing for sediment dynamics remain highly location specific and sediment delivery under warming and wetter climatic conditions appears to be more dependent on sediment connectivity than on the landform processes themselves. Accordingly, assessing climatic forcing upon sediment transfer rates using valley bottom deposits might be misleading and requires particular care.

Future investigations are necessary to better understand the climate forcing signals observed in this alpine setting. First, surface changes and displacements need to be coupled with additional climatic indicators including the frequency of freeze-thaw cycles, intensity of rainfall events, and data on the magnitude of diurnal temperature amplitudes to strengthen the causal link between climate forcing and geomorphic response. Second, a deeper knowledge of permafrost distribution in the area would be beneficial to explain the observed landform behavior at the decadal scale in response to changing climatic conditions. This could be achieved by in situ measurements or modeling approaches. Finally, sediment production rates in the rockwalls represent a key indicator for this type of analysis that could not be derived here and need to be obtained with different approaches.

#### Acknowledgments

This research was supported by the Herbetta Foundation of the University of Lausanne, the Canton Vaud, and the Canton Valais. We would like to thank the University of Fribourg for the collaboration, Jim Chandler and Jean-Michel Fallot for their valuable help during data collection and processing, and Pierre Vacher for providing licenses for the 7D software. Data used in this research are available in <http://ebibalpin.unil.ch> or by contacting the corresponding author. Four anonymous reviewers and an Associate Editor provided constructive and valuable criticism of an earlier draft of this paper.

#### References

- Ballantyne, C. K. (2002), A general model of paraglacial landscape response, *Holocene*, *12*, 371–376.
- Ballantyne, C. K., P. Wilson, D. Gheorghiu, and A. Rodés (2014), Enhanced rock-slope failure following ice-sheet deglaciation: Timing and causes, *Earth Surf. Processes Landforms*, *39*, 900–913.
- Barboux, C., R. Delaloye, and C. Lambiel (2014), Inventorying slope movements in an alpine environment using DInSAR, *Earth Surf. Processes Landforms*, *39*, 2087–2099.
- Bayard, D., M. Stähli, H. Parriaux, and A. Flüeler (2005), The influence of seasonally frozen soil on the snowmelt runoff at two alpine sites in southern Switzerland, *J. Hydrol.*, *309*, 66–84.
- Benn, D., T. Bolch, K. Hands, J. Gulley, A. Luckman, L. Nicholson, D. Quincey, S. Thompson, R. Toumi, and S. Wiseman (2012), Response of debris-covered glaciers in the Mount Everest region to recent warming, and implication for outburst flood hazards, *Earth Sci. Rev.*, *114*, 156–174.
- Bennett, G., P. Molnar, H. Eisenbeiss, and B. McArdell (2012), Erosional power in the Swiss Alps: Characterization of slope failure in the Illgraben, *Earth Surf. Processes Landforms*, *37*, 1627–1640.
- Bennett, G., P. Molnar, B. McArdell, F. Schlunegger, and P. Burlando (2013), Patterns and controls of sediment production, transfer and yield in the Illgraben, *Geomorphology*, *188*, 68–82.
- Beylich, A. A., S. F. Lamoreux, and A. Decaulne (2002), Developing frameworks for studies on sedimentary fluxes and budgets in changing cold environments, *Quaest. Geogr.*, *30*(1), 5–18.
- Bosson, J.-B., P. Deline, X. Bodin, P. Schoeneich, L. Baron, M. Gardent, and C. Lambiel (2014), The influence of ground ice distribution on geomorphic dynamics since the Little Ice Age in proglacial areas of two cirque glacier systems, *Earth Surf. Processes Landforms*, *40*, 666–680.
- Bouët, M. (1985), *Climat et météorologie de la Suisse romande*, 185 p., Payot, Lausanne, Switzerland.
- Brazier, V., M. Kirkbride, and I. Owens (1998), The relationship between climate and rock glacier distribution in the Ben Ohau Range, New Zealand, *Geogr. Ann., Ser. A*, *80*, 193–207.
- Brocklehurst, S. H., and K. X. Whipple (2002), Glacial erosion and relief production in the Eastern Sierra Nevada, California, *Geomorphology*, *42*, 1–24.
- Brunsdon, D., and J. B. Thornes (1979), Landscape sensitivity and change, *Trans. Inst. Br. Geogr.*, *4*, 463–484.
- Carturan, L., et al. (2013), Current behaviour and dynamics of the lowermost Italian glacier (Montasio Occidentale, Julian Alps), *Geogr. Ann., Ser. A*, *95*, 79–96.
- Chandler, J., and M. Cooper (1988), Monitoring of development of landslide using archival photography and analytical photogrammetry, *Land Miner. Surv.*, *6*, 576–584.
- Committee on Challenges and Opportunities in Earth Surface Processes (2010), *Landscapes on the Edge: New Horizons for Research on Earth's Sciences*, Natl. Academies Press, Washington, D. C.
- Davies, M., O. Hamza, and C. Harris (2001), The effect of rise in mean annual temperature on the stability of rock slopes containing ice-filled discontinuities, *Permafrost Periglac. Processes*, *12*, 137–144.

- Delaloye, R., C. Lambiel, R. Lugon, H. Raetzo, and T. Strozzi (2007), Typical ERS InSAR signature of slope movement in a periglacial mountain environment (Swiss Alps), paper presented at ENVISAT Symposium 2007, Montreux, Switzerland, 23–27 April 2007.
- Delaloye, R., et al. (2008), Recent interannual variations of rock glacier creep in the European Alps, in *Proceedings of the Ninth International Conference on Permafrost*, edited by D. L. Kane and M. K. Hinkel, pp. 343–348, Univ. of Alaska, Fairbanks, Alaska.
- Delaloye, R., T. Strozzi, C. Lambiel, S. Mari, A. Stocker, F. Techel, and H. Raetzo (2010), The contribution of InSAR data to the early detection of potentially hazardous active rock glaciers in mountain areas, paper presented at ESA Living Planet Symposium, 28 June–2 July 2010, Bergen, Norway.
- Dissart, O., and O. Jamet (1995), 3D reconstruction of buildings from stereo-images using both monocular analysis and stereomatching: An assessment within the context of cartographic production, in *Proceedings of the Society of Photo-Optical Instrument Engineers, Integrating Photogrammetric Techniques with Scene Analysis and Machine Vision II*, edited by D. M. McKeown and I. J. Dowman, pp. 255–266, SPIE, Wash.
- Dollar, E., and K. Rowntree (1995), Hydroclimatic trends, sediment sources and geomorphic response in the bell river catchment, eastern Cape Drakensberg, South Africa, *S. Afr. Geogr. J.*, 77(1), 21–32.
- Fischer, L., H. Eisenbeiss, A. Kääh, C. Huggel, and W. Haeberli (2011), Monitoring topographic changes in a periglacial high-mountain face using high-resolution DTMs, Monte Rosa East Face, Italian Alps, *Permafrost Periglac. Processes*, 22, 140–152.
- Fischer, L., C. Huggel, A. Kääh, and W. Haeberli (2012), Slope failures and erosion rates on a glacierized high-mountain face under climatic change, *Earth Surf. Processes Landforms*, 38(3), 836–846.
- Ford, J., and B. L. Bedford (1987), The hydrology of Alaskan Wetlands, U.S.A.: A review, *Arct. Alp. Res.*, 19(3), 209–229.
- Forzoni, A., J. Storms, A. Whittaker, and G. de Jager (2014), Delayed deliver from the sediment factory: Modeling the impact of catchment response time to tectonics on sediment flux and fluvio-deltaic stratigraphy, *Earth Surf. Processes Landforms*, 39(5), 689–704.
- Fryirs, K. (2013), (Dis)Connectivity in catchment sediment cascades: A fresh look at the sediment delivery problem, *Earth Surf. Processes Landforms*, 38(1), 30–46.
- Geilhausen, M., D. Morche, J. Otto, and L. Schrott (2013), Sediment discharge from a proglacial zone of a retreating alpine glacier, *Z. Geomorphol.*, 57, 29–53.
- Godon, C., J. L. Mugnier, R. Fallourd, J. L. Paquette, A. Pohl, and J. F. Buoncristiani (2013), The Bosson glacier protects Europe's summit from erosion, *Earth Planet. Sci. Lett.*, 375, 135–147.
- Hales, T. C., and J. J. Roering (2007), Climatic controls on frost cracking and implications for the evolution of bedrock landscapes, *J. Geophys. Res.*, 112, F02033, doi:10.1029/2006JF000616.
- Harvey, A. M. (2001), Coupling between hillslopes and channels in upland fluvial systems: Implications for landscape sensitivity, illustrated from the Howgill Fells, northwest England, *Catena*, 42, 225–250.
- Harvey, A. M. (2002), Effective timescales of coupling within fluvial systems, *Geomorphology*, 44, 175–201.
- Heckmann, T., and W. Schwanghard (2013), Geomorphic coupling and sediment connectivity in an alpine catchment? Exploring sediment cascades using graph theory, *Geomorphology*, 182, 89–103.
- Hözl, M., and W. Haeberli (1995), Simulating the effects of mean annual air-temperature changes on permafrost distribution and glacier size: An example from the Upper Engadin, Swiss Alps, *Ann. Glaciol.*, 21, 399–405.
- Huggel, C., N. Salzmann, S. Allen, J. Caplan-Auerbach, L. Fischer, W. Haeberli, C. Larsen, D. Schneider, and R. Wessels (2010), Recent and future warm extreme events and high-mountain slope stability, *Philos. Trans. R. Soc. A*, 368, 2435–2459.
- Huggel, C., J. J. Clague, and O. Korup (2012), Is climate change responsible for changing landslide activity in high mountains?, *Earth Surf. Processes Landforms*, 37(1), 77–99.
- Hughes, M., P. McDowell, and W. Marcus (2006), Accuracy assessment of georectified aerial photographs: Implications for measuring lateral channel movement in a GIS, *Geomorphology*, 74(1), 1–16.
- Hunt, J. (2002), Floods in a changing climate: A review, *Philos. Trans. R. Soc. A*, 360, 1531–1543.
- Ikeda, A., N. Matsuoka, and A. Kääh (2008), Fast deformation of perennially frozen debris in a warm rock glacier in the Swiss Alps: An effect of liquid water, *J. Geophys. Res.*, 113, F01021, doi:10.1029/2007JF000859.
- Intergovernmental Panel on Climate Change (1990), Seasonal snow cover, ice and permafrost, in *Climate Change: The IPCC Impacts Assessment*, edited by W. J. McG. Tegart, G. W. Sheldon, and D. C. Griffiths, pp. 7.1–7.45, Australian Gov. Publ. Serv., Canberra, Australia.
- Jomelli, V., V. P. Pech, C. Chochillon, and D. Brunstein (2004), Geomorphic variations of debris flows and recent climatic change in the French Alps, *Clim. Change*, 64, 77–102.
- Kääh, A. (2002), Monitoring high-mountain terrain deformation from repeated air- and space borne optical data: Examples using digital aerial imagery and ASTER data, *ISPRS J. Photogramm. Remote Sens.*, 57, 39–52.
- Kääh, A., and M. Vollmer (2000), Surface geometry, thickness changes and flow fields on creeping mountain permafrost: Automatic extraction by digital image analysis, *Permafrost Periglac. Processes*, 11, 315–326.
- Kääh, A., R. Frauenfelder, and I. Roer (2007), On the response of rockglacier creep to surface temperature increase, *Global Planet. Change*, 56, 172–187.
- Keller, F., and H. Gubler (1993), Interaction between snow cover and high mountain permafrost Murtel/Corvatsch, Swiss Alps, in *Proceedings of the Sixth International Conference on Permafrost*, vol. 1, edited by C. Guodong, pp. 332–337, South China Univ. of Technol. Press, Beijing.
- Kellerer-Pirklbauer, A., and V. Kaufmann (2012), About the relationship between rock glacier velocity and climate parameters in Central Austria, *Austrian J. Earth Sci.*, 105(2), 94–112.
- Kirkbride, M. P., and V. Brazier (1995), On the sensitivity of Holocene talus-derived rock glaciers to climate change in the Ben Ohau Range, Southern Alps, New Zealand, *J. Quat. Sci.*, 10, 353–365.
- Kneisel, C., and A. Kääh (2007), Mountain permafrost dynamics within a recently exposed glacier forefield inferred by a combined geomorphological, geophysical and photogrammetrical approach, *Earth Surf. Processes Landforms*, 32, 1797–1810.
- Knox, J. C. (1999), Long-term episodic changes in magnitudes and frequencies of floods in the Upper Mississippi River Valley, in *Fluvial Processes and Environmental Change*, edited by A. G. Brown and T. A. Quine, pp. 255–282, John Wiley, New York.
- Korup, O. (2004), Landslide-induced river channel avulsions in mountain catchments of southwest New Zealand, *Geomorphology*, 63(1–2), 57–80.
- Kundzewicz, Z. W., L. J. Mata, P. Arnell, N. W. Döll, P. Kabat, B. Jimenez, K. A. Miller, T. Oki, Z. Sen, and I. A. Shiklomanov (2007), Freshwater resources and their management, in *Climate Change 2007: Impacts, Adaptation and Vulnerability. Contribution of Working Group II to the Fourth Assessment Report of the Intergovernmental Panel on Climate Change*, edited by M. L. Parry et al., pp. 173–210, Cambridge Univ. Press, Cambridge, U. K.
- Lambiel, C., and E. Reynard (2001), Regional modelling of present, past and future potential distribution of discontinuous permafrost based on a rock glacier inventory in the Bagnes-Hérémence area (Western Swiss Alps), *Norsk. Geogr. Norw. J. Geogr.*, 55, 219–223.

- Lambiel, C., E. Reynard, G. Cheseaux, and R. Lugon (2004), Distribution du pergélisol dans un versant instable, le cas de Tsarmine (Arolla, Evolène, VS), *Bull. Cl. Murithienne*, 122, 89–102.
- Lambiel, C., R. Delaloye, T. Strozzi, R. Lugon, and H. Raetz (2008), ERS InSAR for assessing rock glacier activity, paper presented at 9th International Conference on Permafrost, Fairbanks, Alaska, 29 June–3 July.
- Lambiel, C., B. Maillard, M. Kummert, and E. Reynard (2015), Geomorphological Map of the Hérens Valley (Swiss Alps), *J. Maps*, doi:10.1080/17445647.2014.999135.
- Lambrecht, A., C. Mayer, W. Hagg, V. Popovnin, A. Rezepkin, N. Lomidze, and D. Svanadze (2011), A comparison of glacier melt on debris-covered glaciers in the northern and southern Caucasus, *Cryosphere*, 5, 525–538.
- Lane, S. N., T. D. James, and M. D. Crowell (2000), Application of digital photogrammetry to complex topography for geomorphological research, *Photogramm. Rec.*, 16(95), 793–821.
- Lane, S. N., R. M. Westaway, and D. Murray Hicks (2003), Estimation of erosion and deposition volumes in a large, gravel-bed, braided river using synoptic remote sensing, *Earth Surf. Processes Landforms*, 28, 249–271.
- Lane, S. N., V. Tayefi, S. C. Reid, D. Yu, and R. J. Hardy (2007), Interactions between sediment delivery, channel change, climate change and flood risk in a temperate upland environment, *Earth Surf. Processes Landforms*, 32, 429–446.
- Lane, S. N., P. E. Widdison, R. E. Thomas, P. J. Ashworth, J. L. Best, I. A. Lunt, G. H. Sambrook Smith, and C. J. Simpson (2010), Quantification of braided river channel change using archival digital image analysis, *Earth Surf. Processes Landforms*, 35, 971–985.
- Matsuoka, N. (2008), Frost weathering and rockwall erosion in the southeastern Swiss Alps: Long-term (1994–2006) observations, *Geomorphology*, 99, 353–368.
- Meteosuisse (2014), Climate today: Trends in Switzerland, *Tech. Rep.*, Federal Office of Meteorology and Climatology Meteoswiss, Zürich. [Available at [www.meteosuisse.admin.ch](http://www.meteosuisse.admin.ch).]
- Micheletti, N., J. H. Chandler, and S. N. Lane (2015), Application of archival aerial photogrammetry to quantify climate forcing of alpine landscapes, *Photogramm. Rec.*, 30(150), 143–165.
- Montgomery, D. R., and S. C. Stover (2001), Channel change and flooding, Skokomish River, Washington, *J. Hydrol.*, 243(3–4), 272–286.
- Müller, J., I. Gärtner-Roer, R. Kenner, P. Thee, and D. Morche (2014), Sediment storage and transfer on a periglacial mountain slope (Corvatsch, Switzerland), *Geomorphology*, 218, 35–44.
- Oliva, M., and J. Ruiz-Fernandez (2015), Coupling patterns between para-glacial and permafrost degradation responses in Antarctica, *Earth Surf. Processes Landforms*, 40, 1227–1238, doi:10.1002/esp.3716.
- Pelto, M. S., and C. Hedlund (2001), Terminus behavior and response time of North Cascade Glaciers, Washington, USA, *J. Glaciol.*, 47(158), 497–506.
- PERMOS (2013), Permafrost in Switzerland 2008/2009 and 2009/2010, in *Glaciological Report (Permafrost) No. 10/11 of the Cryospheric Commission of the Swiss Academy of Sciences*, edited by J. Noetzli, 80 pp., PERMOS Off., Dep. of Geogr., Univ. of Zurich, Winterthurerstrasse, Zurich.
- Phillips, J. D. (2003), Sources of nonlinearity and complexity in geomorphic systems, *Prog. Phys. Geogr.*, 27(1), 1–23.
- Phillips, J. D. (2009), Changes, perturbations, and responses in geomorphic systems, *Prog. Phys. Geogr.*, 33(1), 17–30.
- Reynard, E., C. Lambiel, and S. N. Lane (2012), Climate change and integrated analysis of mountain geomorphological systems, *Geogr. Helv.*, 1–2, 5–14.
- Roer, I., A. Kääh, and R. Dikau (2005), Rockglacier kinematics derived from small-scale aerial photography and digital airborne pushbroom imagery, *Z. Geomorphol.*, 49, 73–87.
- Roer, I., W. Haeberli, M. Avian, V. Kaufmann, R. Delaloye, C. Lambiel, and A. Kääh (2008), Observations and considerations on destabilizing active rock glaciers in the European Alps, in *Proceedings of the 9th International Conference on Permafrost*, edited by D. L. Kane and K. M. Hinkel, pp. 1505–1510, Univ. of Alaska, Fairbanks, Alaska.
- Rumsby, B. T., and M. G. Macklin (1994), Channel and floodplain response to recent abrupt climate change: The tyne basin, northern England, *Earth Surf. Processes Landforms*, 19, 499–515.
- Schaepli, B., and M. Huss (2011), Integrating point glacier mass balance observations into hydrologic model identification, *Hydrol. Earth Syst. Sci.*, 15, 1227–1241.
- Schaepli, B., B. Hingray, M. Niggli, and A. Musy (2005), A conceptual glacio-hydrological model for high mountainous catchments, *Hydrol. Earth Syst. Sci.*, 9, 95–109.
- Schwab, M., D. Rieke-Zapp, H. Scheider, M. Liniger, and F. Schlunegger (2008), Landsliding and sediment flux in the Central Swiss Alps: A photogrammetric study of the Schimbrig landslide, Entlebuch, *Geomorphology*, 97, 392–406.
- Shroder, J., M. Bishop, L. Copland, and V. Sloan (2000), Debris-covered glaciers and rock glaciers in the Nanga Parbat Himalaya, Pakistan, *Geogr. Ann., Ser. A*, 82, 17–31.
- Staines, K. E. H., J. L. Carrivick, F. S. Tweed, A. J. Evans, A. J. Russell, T. Johannesson, and M. Roberts (2015), A multi-dimensional analysis of pro-glacial landscape change at Sólheimajökull, southern Iceland, *Earth Surf. Processes Landforms*, 40, 809–822.
- Takeuchi, Y., R. B. Kayastha, and M. Nakawo (2000), Characteristics of ablation and heat balance in debris-free and debris-covered areas on Khumbu Glacier, Nepal Himalayas, in the pre-monsoon season, in *Debris-Covered Glaciers*, vol. 264, edited by M. Nakawo, C. F. Raymond, and A. Fountain, pp. 53–61, IAHS, Wallingford, U. K.
- Thomas, M. F. (2001), Landscape sensitivity in time and space—An introduction, *Catena*, 42, 83–98.
- Tobin, C., L. Nicotina, M. B. Parlange, A. Berne, and A. Rinaldo (2011), Improved interpolation of meteorological forcings for hydrologic applications in a Swiss Alpine region, *J. Hydrol.*, 401, 77–89.
- Vacher, P., S. Dumoulin, F. Morestin, and S. Mguil-Touchal (1999), Bidimensional strain measurement using digital images, *Proc. Inst. Mech. Eng.*, 213(8), 811–817.
- Walstra, J., N. Dixon, and J. Chandler (2007), Historical aerial photographs for landslide assessment: Two case histories, *Q. J. Eng. Geol. Hydrogeol.*, 40(4), 315–332.
- Wangenstein, B., A. Gudmundsson, T. Eiken, A. Kääh, H. Farbrót, and B. Etzelmüller (2006), Surface displacements and surface age estimates for creeping slope landforms in Northern and Eastern Iceland using digital photogrammetry, *Geomorphology*, 80, 59–79.
- Warner, R. F. (1987), Spatial adjustment to temporal variations in flood regime in some Australian Rivers, in *River Channel Changes, Environment and Process*, edited by K. Richards, pp. 14–40, Basil Blackwell, Oxford, England.
- WAV Laboratory of Hydraulics, Hydrology and Glaciology (2013), *Glaciological reports (1881–2009)*. The Swiss Glaciers—Yearbooks of the Cryospheric Commission of the Swiss Academy of Sciences (SCNAT) published since 1964, Zürich: ETH. [Available at [glaciology.ethz.ch/swiss-glaciers](http://glaciology.ethz.ch/swiss-glaciers).]